JOURNAL OF MATERIALS SCIENCE 31 (1996) 453–461

The effect of stress triaxiality and strain-rate on the fracture characteristics of ductile metals

M. S. MIRZA, D. C. BARTON
Department of Mechanical Engineering, University of Leeds, LS2 9JT, UK
P. CHURCH
DRA, Fort Halstead, Sevenoaks, Kent, TN14 7BP, UK

Notched tensile tests have been carried out on three common metals (pure iron, mild steel and aluminium alloy BS1474) over a wide range of strain-rates (10^{-3} to $10^{4}\ s^{-1}$) and the strain-to-failure measured. The ductility of all three materials was found to be strongly dependent on the level of stress triaxiality in the specimen, this dependency being greatest for the ferrous materials and least for the aluminium alloy. No significant effect of strain-rate could be ascertained from the experimental results provided fracture remained fully ductile. However, for mild steel, a transition to a brittle fracture mode was observed for a given level of stress triaxiality as the strain-rate was increased. Numerical simulations of the experiments have been used to derive constants of a semi-empirical fracture model from the measured results. This model was found to give reasonable predictions of fracture over the range of conditions investigated.

1. Introduction

Many studies have been carried out to determine the plasticity characteristics of ductile metals at high strain-rates. Such information is of vital importance in vehicle crashworthiness studies, ballistic impact simulations and high rate metal forming operations. Common test techniques include the split Hopkinson pressure bar and the Taylor cylinder impact test. Results are normally presented in the form of empirical or semi-empirical relations giving the material flow stress (σ) as a function of effective plastic strain (ε), plastic strain-rate ($\dot{\varepsilon}$) and temperature (T). For example, the well-known Johnson–Cook relation [1] takes the form

$$\sigma = (A + B\varepsilon^n)(1 + C\ln\dot{\varepsilon})(1 - T^m) \quad (1)$$

where A, B, C, n and m are material constants. A more theoretical approach based on the micromechanics of dislocation motion is taken by Armstrong and Zerilli [2] who have formulated the following expressions for fcc and bcc metals, respectively:

$$\sigma = \Delta\sigma_g + C_1 l^{-1/2} + C_2\varepsilon^{1/2}\exp[(-C_3 + C_4\ln\dot{\varepsilon})T] \quad (2)$$

$$\sigma = \Delta\sigma_g + C_1 l^{-1/2} + C_2\exp[(-C_3 + C_4\ln\dot{\varepsilon})T] + C_5\varepsilon^n \quad (3)$$

where $\Delta\sigma_g$ is the stress due to solute, l is the average grain size and C_1–C_5 are material constants. The latter has been modified recently for pure iron by Goldthorpe [3] to give the following form which has been shown to be applicable for strain-rates up to $3 \times 10^4\ s^{-1}$ and temperatures up to 600 K

$$\sigma = C_1 + C_2\exp[(-C_3 + C_4\ln\dot{\varepsilon})T] + (C_5\dot{\varepsilon}^n)(C_6 - C_7 T) \quad (4)$$

where C_1–C_7 and n are material constants.

In addition to plasticity considerations, ultimate material failure under impact loading conditions is of considerable importance. Although much effort has been directed at measuring the brittle fracture properties of materials at high rates of loading, less attention has been paid to the strain-rate sensitivity of the ductile fracture process. This process is characterized by the nucleation, growth and eventual coalescence of microvoids within the material and is known to be strongly dependent on the triaxial state of stress at the site of failure initiation. For example, the analysis of the growth of an initially spherical hole by Rice and Tracey [4] showed that the rate of change of the mean hole radius R strongly depends upon the stress triaxiality (measured as the ratio of hydrostatic tension or mean stress σ_m to the von Mises effective stress σ_e)

$$\frac{dR}{R} = 0.28 d\varepsilon \exp\left(\frac{3\sigma_m}{2\sigma_e}\right) \quad (5)$$

where dR is the change in hole radius for a given increment of plastic strain $d\varepsilon$. Hancock and Mackenzie [5] tested three rolled, low alloy, quenched and tempered steels and found the ductility (measured as the effective plastic strain at fracture in a simple tensile test, ε_f) to be related to the stress triaxiality

as follows:

$$\varepsilon_f = \alpha \exp\left(-\frac{3\sigma_m}{2\sigma_e}\right) \quad (6)$$

where α is a material constant.

Since the state of stress is dependent on the material plasticity which itself is sensitive to strain-rate, it is likely that the ductility may also vary according to the rate of loading. Knowledge of such an effect is of importance in understanding and simulating ductile fracture in any of the high strain-rate situations mentioned above. Indeed, Johnson and Cook [6] have proposed a relation for fracture strain as a function of stress triaxiality, strain-rate and temperature which has been made available in one of the principal computer codes used for high strain-rate simulations (DYNA [7, 8]). This relation has the following form:

$$\varepsilon_f = [D_1 + D_2 \exp(D_3 \sigma_m/\sigma_e)]\,[1 + D_4 \ln\dot{\varepsilon}]\,[1 + D_5 T^*] \quad (7)$$

where D_1–D_5 are again material constants and T^* is the homologous temperature.

The present paper reports a comprehensive experimental study designed to investigate the combined effects of state-of-stress and strain-rate on the strain-to-failure of common metals (mild steel, pure iron and aluminium alloy) which are known to be ductile under normal conditions. The state-of-stress was varied by machining notches of pre-determined dimensions in plain cylindrical tensile specimens. The strain-rate was varied by carrying out tensile tests at both quasi-static rates and dynamically at strain-rates up to $10^4\ s^{-1}$ using a unique impact tensile test facility known as the "flying wedge". Raw results are the measured plastic strain after fracture along with details of the loading conditions, the time to fracture and micrographs illustrating the mode of failure. In order to correctly interpret these data, the non-linear finite element codes DYNA2D and NIKE2D have been used to predict the exact conditions of stress and strain at the expected site of fracture initiation. The results are then used to determine the constants of empirical relations such as Equation 7. The relations obtained are in turn employed in further numerical simulations of the dynamic tensile test to predict the strain and time to failure for comparison with experiment in order to validate the relations obtained and the numerical techniques employed.

2. Experimental investigation

2.1. Materials and test specimens

A detailed experimental tensile test programme was carried out on three materials: mild steel (0.5% carbon), specially processed pure Remko iron (known as AQ85 iron) and aluminium alloy (BS1474 TF-HE30). To obtain a range of stress triaxiality factor, notches of different notch severity were machined in plain cylindrical tensile specimens. Two sizes of test specimens were used in the present study: (a) 15 mm gauge diameter with M20 threaded ends; (b) 9 mm gauge diameter with M12 threaded ends. The nominal dimensions and range of notch profile radius for both M20 and M12 threaded specimens are shown in Fig. 1. Both sizes of specimen were used for tests on mild steel to study the effect of specimen size on the ductility. Pure AQ85 iron was tested using M12 specimens with four different notch profile radii while M20 threaded specimens were used for aluminium alloy with five different notches.

2.2. Test techniques

At least three tests were carried out at each of four strain-rates ranging from quasi-static to $10^4\ s^{-1}$ for all notch profile radii. Quasi-static tests were performed using a 200 kN Dartec servohydraulic tensile testing

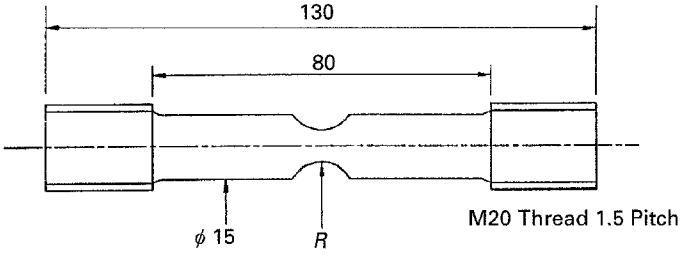

(a)

	Notch Profile Radius R
1.	8.0 mm
2.	4.0 mm
3.	2.0 mm
4.	1.0 mm
5.	0.5 mm

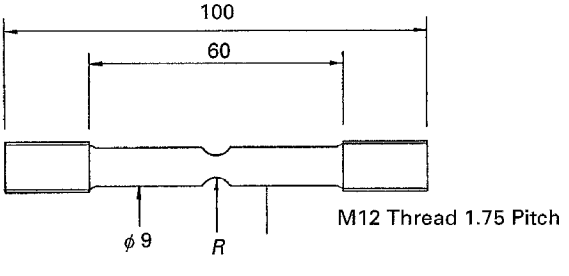

(b)

	Notch Profile Radius R
1.	4.0 mm
2.	2.0 mm
3.	1.0 mm
4.	0.5 mm

Figure 1 Geometry and dimension of (a) M20 and (b) M12 threaded tensile specimens.

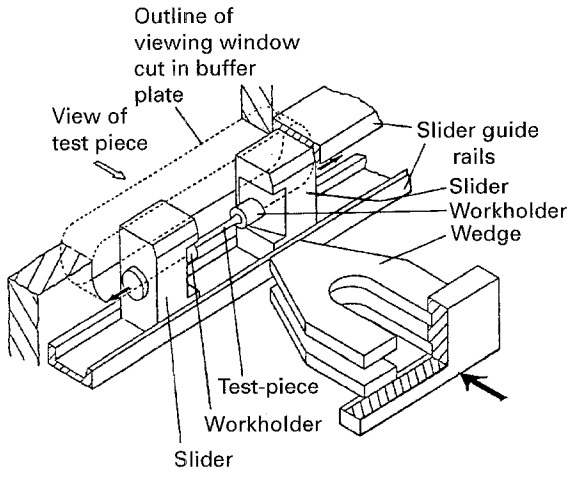

Figure 2 Schematic diagram of dynamic tensile testing machine flying wedge.

machine. The high strain-rate tests were performed on the so-called "flying wedge" dynamic tensile testing machine. This is capable of imparting simultaneous symmetrical loading at both ends of a tensile specimen over a wide range of loading speeds, Fig. 2. It is based on the simple idea of holding a tensile specimen between a pair of sliders with chamfered faces which are impacted upon by a wedge of matching semi-angles travelling at high velocity fired from a gas gun, thereby subjecting the specimen to very high speed uniaxial tension from both ends. By varying the speed of the impacting wedge (3–15 ms^{-1}) and the slider and wedge semi-angles (5, 28 and 45° semi-angled components are available), a wide range of strain-rates from $10^2\ s^{-1}$ to in excess of $10^4\ s^{-1}$ can be achieved.

During each test on the flying wedge, the impacting wedge velocity was measured carefully and with good accuracy just before impact using a photographic fringe technique. The deformation of the specimen during a test can also be monitored using high speed cameras. For most tests foil strain gauges were mounted on the specimen and on the specimen holders to record the axial strain and load on the specimen and to indicate the start of specimen loading. In addition fracture times were recorded by passing a small current through the specimen. When the specimen breaks the flow of current is interrupted thereby allowing the moment of fracture to be determined accurately for estimation of the mean strain-rate and validation of the fracture model predictions.

2.3. Results

After each test, the minimum diameter of the fractured specimen was measured carefully at at least ten positions using a Nikon profile projector. The effective plastic strain at fracture (ε_f) was calculated as:

$$\varepsilon_f = 2\ln\left(\frac{d}{d_f}\right) \tag{8}$$

where d and d_f are the mean initial and final root diameters, respectively. Average strain-rates ($\dot{\varepsilon}$) were calculated by dividing ε_f by the measured fracture time (t_f). This method only provides an average strain-rate over the whole test since the actual strain-rate varies with both time and position within the specimen.

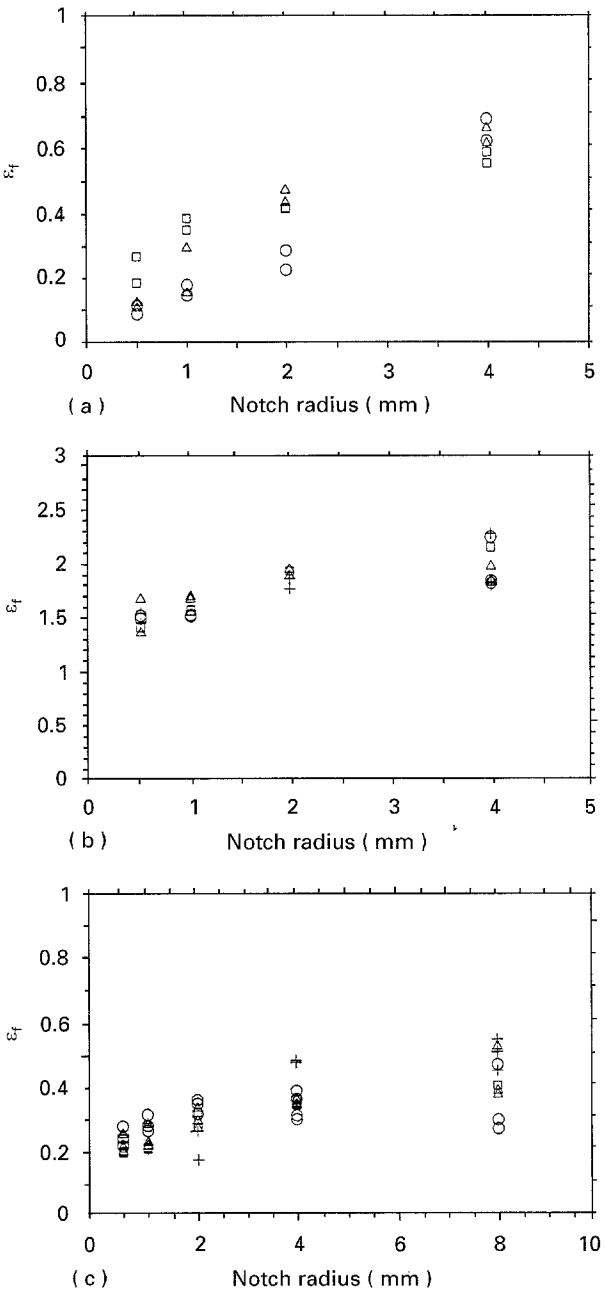

Figure 3 Effective plastic strain at failure versus notch radius for (a) mild steel, (b) AQ85 pure iron and (c) aluminium alloy. (a) ○ $2\times10^3\ s^{-1}$, △ $5\times10^2\ s^{-1}$, □ $8\times10^{-2}\ s^{-1}$; (b) + $1.5\times10^4\ s^{-1}$, ○ $9.0\times10^3\ s^{-1}$, △ $3.3\times0^{-2}\ s^{-1}$, □ $8.0\times10^{-2}\ s^{-1}$; and (c) + $2.7\times10^3\ s^{-1}$, ○ $1.5\times10^3\ s^{-1}$, △ $2.2\times10^2\ s^{-1}$, □ $3.5\times10^{-2}\ s^{-1}$.

Fig. 3 shows the raw data plotted in terms of effective plastic strain at fracture versus notch profile radius. The expected general tendency for fracture strain to increase with increasing notch profile radius is clear but there is a lot of scatter in the results and it is difficult to identify other trends at this stage.

Fractographic examination of the fractured surfaces of mild steel using a CAMSCAN scanning electron microscope (SEM) revealed that the fracture mechanism was strongly dependent on the notch radius and also to some degree on strain-rate. The effect of notch radii can be seen very clearly from Fig. 4 which shows

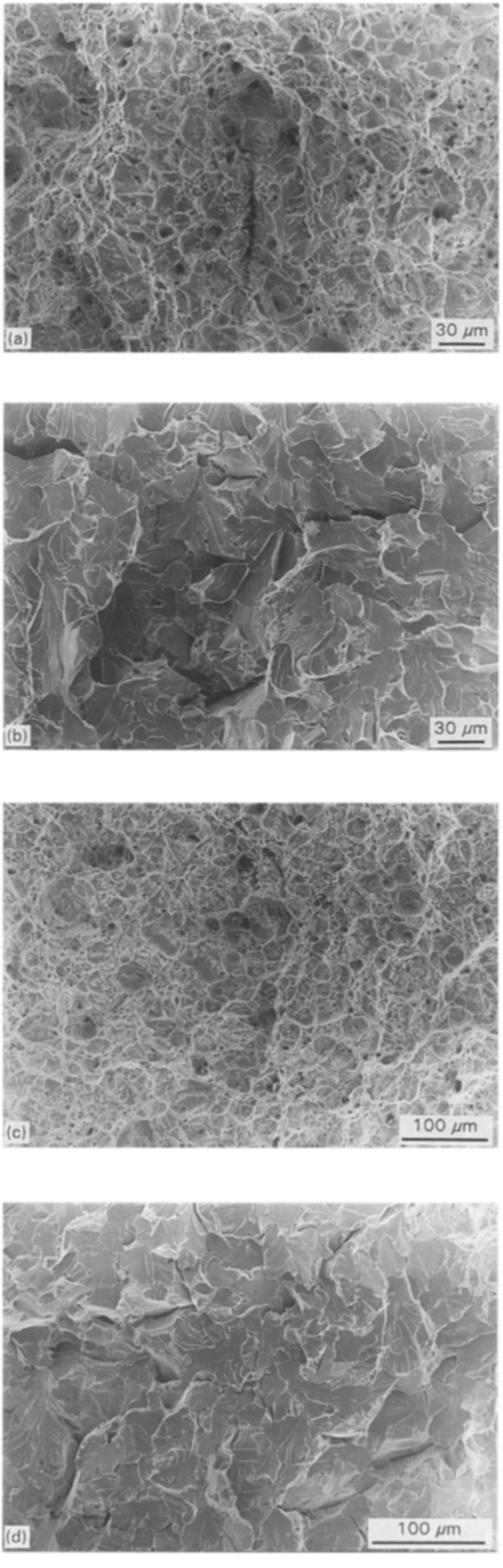

Figure 4 SEM micrographs of mild steel, (a) and (b) 4 and 0.5 mm notch specimen tested with 28° wedge impacting at 10 ms^{-1} (c) and (d) 4 mm and 0.5 mm notch specimen tested quasi-statically.

TABLE I Change of failure mode from ductile to brittle for mild steel

Notch radius (mm)	28° slider-wedge ($2.5 \times 10^3 s^{-1}$)	5° slider-wedge ($3.5 \times 10^2 s^{-1}$)	Quasi-static ($8 \times 10^{-2} s^{-1}$)
4	D	D	D
2	B	D	D
1	B	B	D
0.5	B	B	B

D = ductile fracture; B = brittle fracture.

electron micrographs for 4 and 0.5 mm notch profiles tested at high rates with the 28° wedge fired at 10 ms^{-1} (equivalent to an average strain-rate of about 3×10^3 s^{-1}) and at quasi-static rates. The 4 mm notch specimen for both strain-rates (Fig. 4a and c) displays a dimpled fracture surface representing ductile fracture whereas, for the 0.5 mm notch profile (Fig. 4b and d) the surface consists of flat facets containing large multiple cracks, representing a brittle fracture mode. The results of the fractographic examinations for this material are summarized in Table I. For example, a transition from a purely ductile fracture mode for the 4 mm notch to that of cleavage fracture mode for the 2, 1 and 0.5 mm notch radii tested with the 28° slider-wedge was evident. Table I shows that this ductile–brittle transition depends not only upon the notch profile radius (i.e. the stress triaxiality) but also on the strain-rate: for the 28° slider-wedge (average strain-rate of 2.5×10^3 s^{-1}), the transition to brittle fracture takes place for the 2, 1, and 0.5 mm notches; for the specimens tested with the 5° slider-wedge (average strain-rate of 3.5×10^2 s^{-1}), the brittle fracture occurs for the 1 and 0.5 mm notches; whilst, for the quasi-static rates, only the 0.5 mm notch specimens fail in a brittle manner.

The above results for mild steel are similar to those previously obtained for as-received (i.e. not specially processed) Remko iron [9]. In contrast, examination of the fractured surfaces of the AQ85 pure iron revealed no apparent change in the fracture mode even at the highest rate of 1.5×10^4 s^{-1} and with the smallest of the notch profiles. The primary mode of failure for all conditions was ductile, the fracture surface consisting of equiaxed dimples near the centre and non-equiaxed dimples near the surface of the specimen. However, it was noticed that the dimples decrease in number and become larger in size with decreasing notch profile radius (i.e. increasing stress triaxiality) as shown in Fig. 5. This dependence of void size on stress triaxiality is consistent with most theories of ductile failure in which the rate of void nucleation and growth is assumed to be directly proportional to the stress triaxiality.

Fractographic examination of the aluminium alloy reveal that the fracture mode is purely ductile for all the five notch profiles tested at different strain-rates. Even at the lowest fracture strain of only about 0.2 the failure mode is ductile. No significant change in void size was observed for the different notch profile radii. These results suggest that the effect of stress triaxiality is less pronounced for this material and again that the

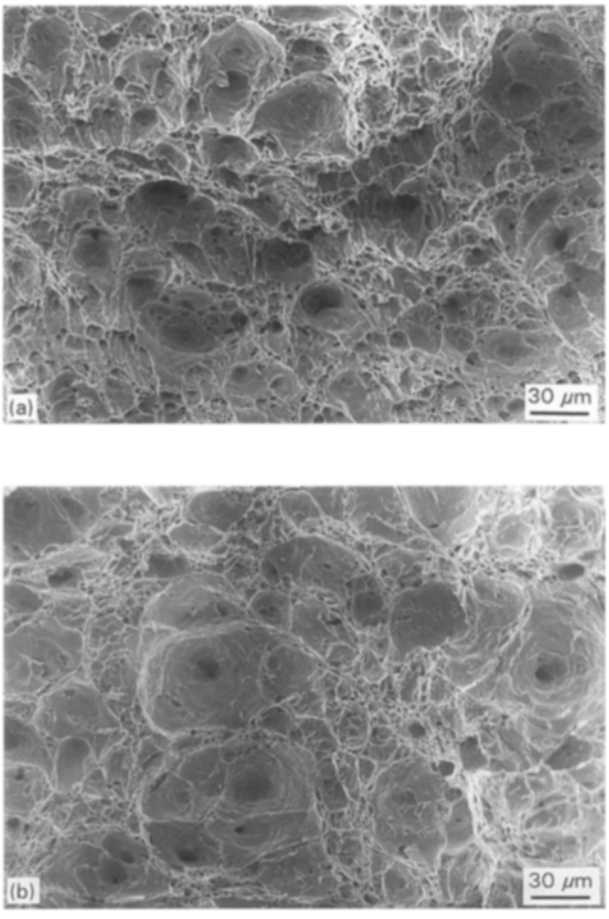

Figure 5 SEM micrographs of AQ85 pure iron tested with 45° wedge impacting at 10 ms^{-1} (a) 4 mm notch specimen and (b) 0.5 mm notch specimen.

fracture mechanism is not influenced by strain-rate over the range of conditions tested.

3. Numerical simulations

The stress triaxiality is an important parameter which has been recognized by McClintock [10] and Rice and Tracey [4] to control the void growth rate leading to ductile failure. To better understand these effects, accurate estimates of the state of stress and strain-rate in the specimen are necessary. Many investigations have used the approximate solution of Bridgman's analysis [11] to obtain estimates of the stress triaxiality parameter σ_m/σ_e in a notch tensile specimen [5, 9, 12]. However, it has been argued that the application of Bridgman's analysis, which was originally performed for a naturally necking tensile specimen, to the pre-notched tensile specimens may not be without errors [13–15].

In the present work finite element analyses of the notched tensile specimens have been used to get more accurate estimates of the state of stress and strain-rate at the site of fracture initiation. To estimate the true conditions in the notched tensile specimens at different rates of loading, a two-dimensional axisymmetric model is quite adequate and also very efficient. However, the application of the correct loading conditions also is very important. The velocity–time loading history to which the ends of a tensile specimen are

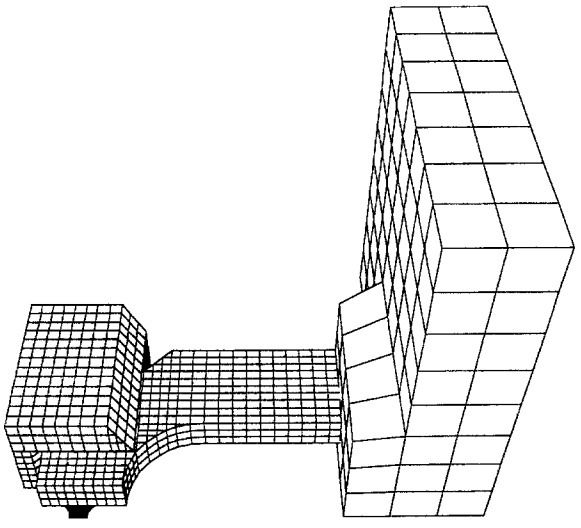

Figure 6 Three-dimensional finite element model of flying wedge tensile testing machine.

subjected when tested on the flying wedge cannot at present be measured with sufficient accuracy because of the very rapid rise time and short total test duration. However, the velocity of the wedge as it impacts the sliders is measured with a high degree of accuracy. Hence the complete flying wedge experiment was modelled using the three-dimensional explicit finite element code DYNA3D [8], a typical mesh being shown in Fig. 6. All three sets of slider-wedge combinations (i.e. semi angles of 5, 28 and 45°) were modelled with both M20 and M12 threaded end specimens at different wedge impact velocities as measured during a test. The velocity–time loading history at the end of the tensile specimen predicted by DYNA3D was then used as an input boundary condition for the detailed axisymmetric modelling of the specimen. This approach not only enables accurate two-dimensional simulations of the test conditions but also allows very fine axisymmetric meshes to be used with reasonable run times to obtain good accuracy. The axisymmetric finite element meshes used for the M12 threaded end specimens with different notch profile radii are shown in Fig. 7.

The two-dimensional explicit wave propagation finite element code DYNA2D [7] was used for the high rate axisymmetric simulation of the notched tensile test. The quasi-static simulations were performed using the implicit two dimensional code NIKE2D [16] and with the measured displacement boundary conditions from the Dartec test. For AQ85 pure iron, the constitutive relation specified was the modified Zerilli–Armstrong relation determined for this type of iron by Goldthorpe (Equation 4), with the following constants: $C_1 = 50$ MPa, $C_2 = 1130$ MPa, $C_3 = -0.00515\,K^{-1}$, $C_4 = 0.000262\,°K^{-1}$, $C_5 = 357$ MPa, $C_6 = 1.13$, $C_7 = 0.000445\,K^{-1}$ and $n = 0.52$. For mild steel and aluminium alloy, in the absence of any rate dependent constitutive relation, a simple isotropic-elastic-plastic-hydrodynamic material model with linear strain hardening was used, with yield stresses of 580 and 340 MPa and hardening moduli of 390 and 280 MPa, respectively. These

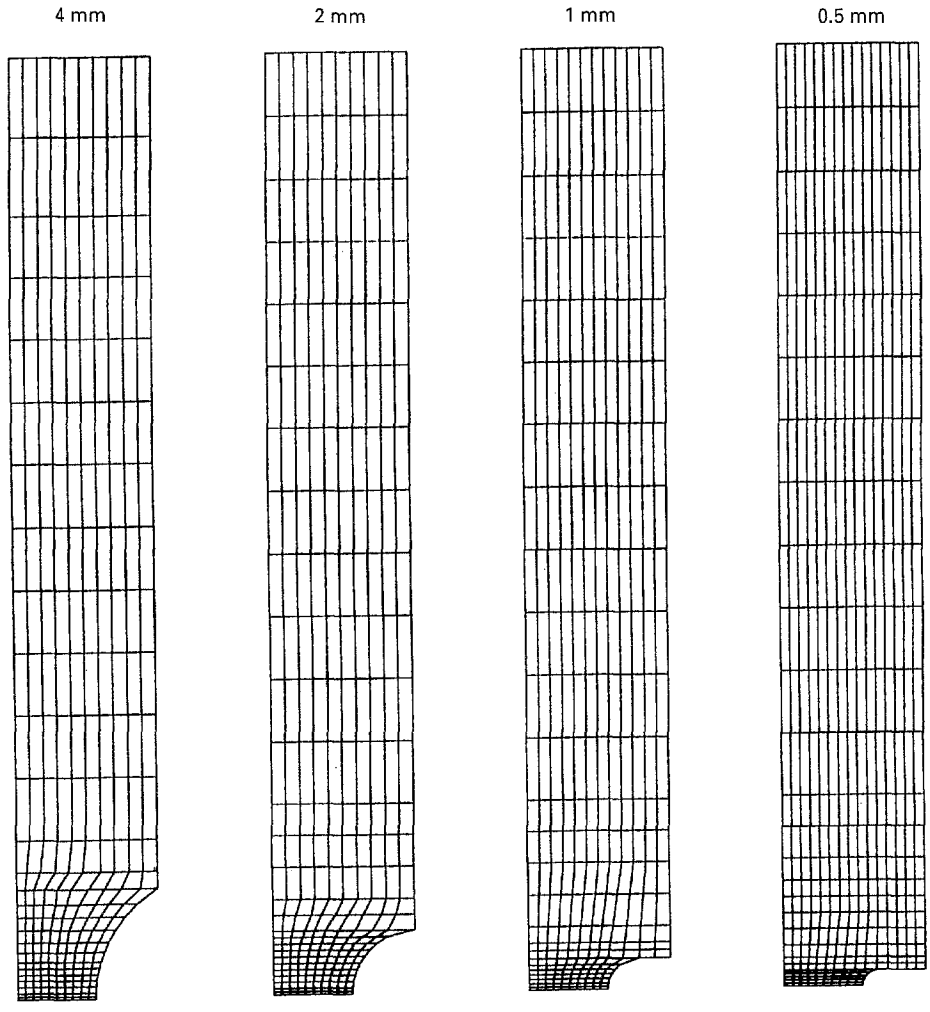

Figure 7 Axisymmetric DYNA2D meshes for M12 specimens.

parameters were obtained from careful quasi-static plain (i.e. unnotched) tensile tests up to failure using a special photographic technique to record the plastic strains.

Variations of the stress triaxiality parameter σ_m/σ_e at the centre of the specimen with effective plastic strain (Equation 8) as predicted by the numerical simulations of AQ85 iron with the four notch profile radii at an average strain-rate of $10^4\ s^{-1}$ are shown in Fig. 8. It can be seen that σ_m/σ_e for the smaller notch radii tends to decrease with increasing effective plastic strain. This is due to the effective blunting of the initially quite sharp notch as deformation proceeds. In contrast, σ_m/σ_e for the larger notch radii (4 and 2 mm) increases with strain. This is thought to be due to secondary neck formation near the centre of the notch which could be clearly seen on both experimental and numerical deformed profiles. The net result of these trends is that, near the fracture strain for pure iron of approximately 2, the curves for the four notch profiles have converged and there is far less range in σ_m/σ_e than might be expected from the initial profile radii. However, for the less ductile mild steel and aluminium, the failure strains are around 1 for which a greater range of σ_m/σ_e is maintained (the σ_m/σ_e versus effective strain curves for these materials were similar to those shown in Fig. 8).

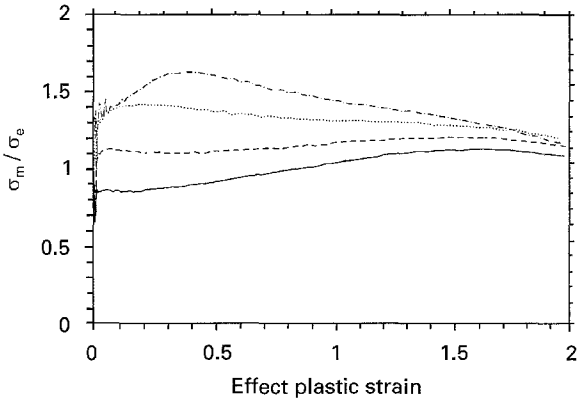

Figure 8 Variation of σ_m/σ_e with effective plastic strain for pure iron with 45° wedge impacting at $10\ ms^{-1}$. 4 mm ——; 2 mm - - - -; 1 mm .....; and 0.5 mm —·—·—.

The combined experimental and numerical results for mild steel, pure iron and aluminium alloy are shown in Fig. 9, respectively, in terms of the measured effective plastic strain at failure versus the maximum stress triaxiality at this failure strain as predicted by the numerical simulations. For mild steel the results are differentiated both in terms of strain-rate and specimen size, Fig. 9a. It can be seen that there is no systematic difference between the M20 and M12

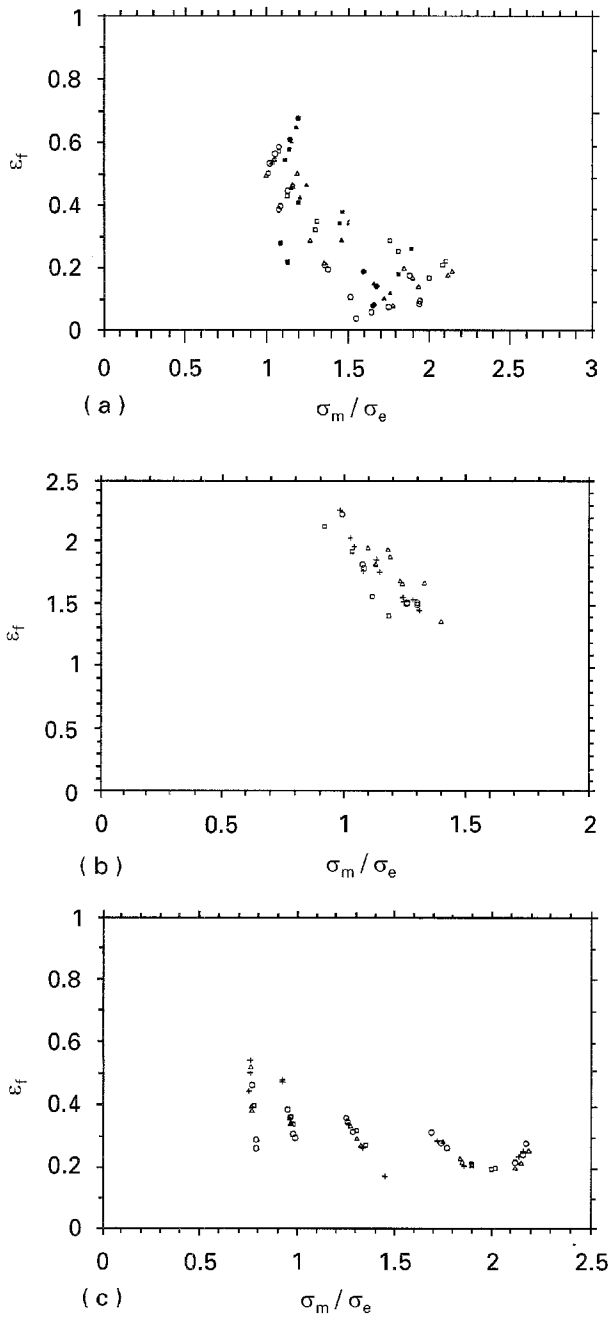

Figure 9 Average effective plastic strain at failure versus σ_m/σ_e for (a) mild steel, (b) AQ85 pure iron and (c) aluminium alloy. (a) M20–$2.5\times10^3\,s^{-1}$ ○, M20–$3.5\times10^2\,s^{-1}$ △, M20–$2\times10^{-2}\,s^{-1}$ □, M12–$2.0\times10^3\,s^{-1}$ ●, M12–$5.0\times10^2\,s^{-1}$, ▲, M12–$8\times10^{-2}\,s^{-1}$ ■; (b) $1.5\times10^4\,s^{-1}$ +, $9.0\times10^3\,s^{-1}$ ○, $3.3\times10^2\,s^{-1}$ △, $8.0\times10^{-2}\,s^{-1}$ □; and (c) $2.7\times10^3\,s^{-1}$ +, $1.5\times10^3\,s^{-1}$, ○, $2.2\times10^2\,s^{-1}$ △, $3.5\times10^{-2}\,s^{-1}$ □.

specimen results which indicates that the specimen size does not significantly affect the measured ductility. A very strong influence of σ_m/σ_e on the measured strain is apparent as expected. Small notch radii specimens tested dynamically have very low failure strains because of the ductile–brittle transition described above. However, apart from this transition, no systematic effect of strain-rate can be seen. For pure AQ85 iron, Fig. 9b shows the strong influence of σ_m/σ_e on the failure strain but no obvious effect of strain-rate. Even at the highest rates ($2\times10^4\,s^{-1}$), the strains remain high which confirms that the failure is purely ductile through the range of strain-rates tested. Results for aluminium are shown in Fig. 9c. As for mild steel the ductility of the material is low. However, the effect of σ_m/σ_e on failure strain is less pronounced for aluminium (as suggested by the fractographic studies). Again no obvious strain-rate effect is apparent from these results.

4. Semi-empirical fracture model

Data from the experiments and from the numerical simulations at different strain-rates and levels of stress-triaxiality have been used to derive constants for semi-empirical fracture models for the three materials of the form shown in Equation 7. Only a limited number of constants are required for this model, unlike the more complicated nucleation and growth (NAG) ductile fracture models [17, 18].

The results discussed above for mild steel, AQ85 iron and aluminium alloy have shown strong dependence of strain to failure on σ_m/σ_e but no discernible trend between results at different strain-rates. Also the tests were performed at room temperature. Therefore it is reasonable to assume the constants D_4 and D_5 of Equation 7 are both zero under these conditions. The first term in the equation, which follows the form presented by Hancock and Mackenzie [5], essentially says that the strain to fracture decreases exponentially as the stress triaxiality increases. The constant D_1 implies a finite strain to failure even at very high values of σ_m/σ_e. In the absence of any data at σ_m/σ_e values greater then 2.5 and in the light of very low element strains at failure for only moderate σ_m/σ_e in the case of mild steel, the constant D_1 was also set to zero. The remaining two constants D_2 and D_3 were found by fitting curves of the correct form to the maximum local strain versus σ_m/σ_e data, both quantities as predicted by the numerical simulations for the centre-most element at the measured diametral failure strain (failure is assumed to always initiate at the centre of the neck). These data along with the fitted fracture loci are shown in Fig. 10 and the derived constants are given in Table II for mild steel, AQ85 pure iron and aluminium alloy, respectively. It is interesting that the value of D_3 predicted for pure iron is very close to the factor of 1.5 assumed by Hancock and Mackenzie [5].

Simulations of the notched tensile tests were repeated for the mild steel, AQ85 iron and aluminium alloy using the above fracture model with the newly derived constants. The fracture criterion available in DYNA2D uses the concept of an accumulative damage parameter D to account for the path dependency of fracture. The damage is an element is defined as:

$$D = \sum \frac{\Delta\varepsilon}{\varepsilon_f} \tag{9}$$

where $\Delta\varepsilon$ is the increment of effective plastic strain during an integration cycle (time step) and ε_f is the effective strain for fracture under the current conditions of strain-rate, temperature and σ_m/σ_e. Fracture is assumed to occur when the damage parameter reaches unity.

For the present work, an element deletion scheme was developed and coded into the Leeds version of DYNA2D whereby elements are removed from the mesh when $D = 1$. The axisymmetric simulations were

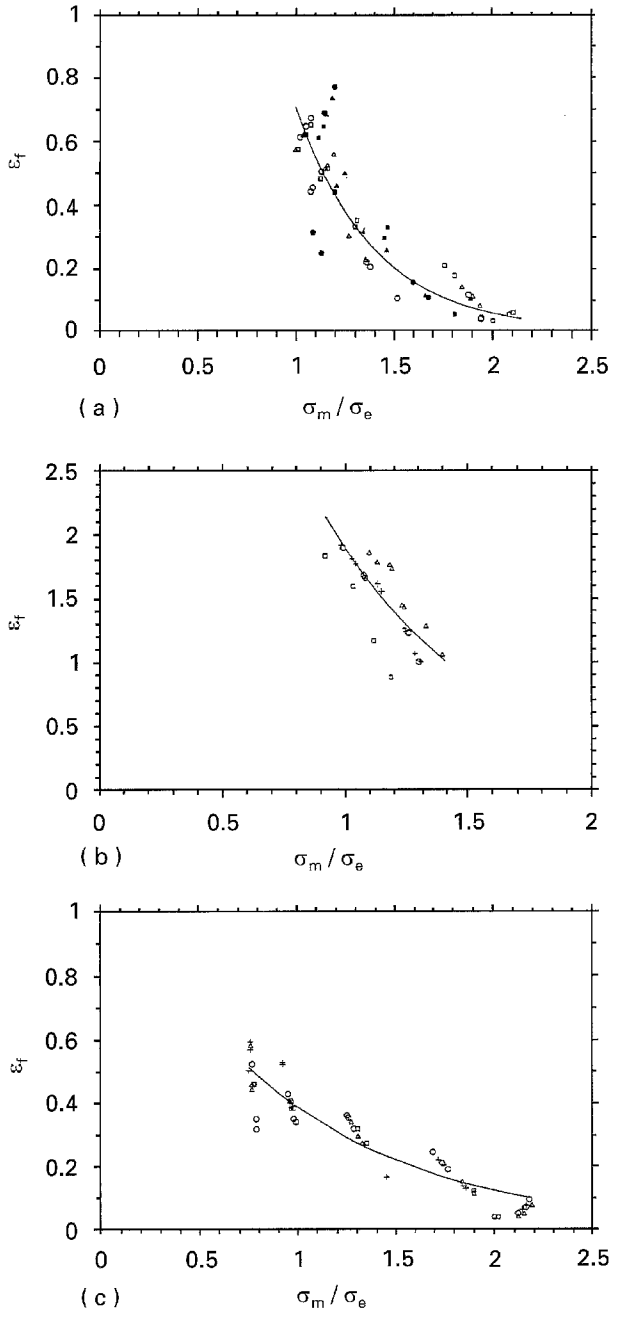

Figure 10 Maximum local effective plastic strain versus σ_m/σ_e for (a) mild steel, (b) AQ85 pure iron and (c) aluminium alloy. (a) M20–$2.5\times10^3\,s^{-1}$ ○, M20–$3.5\times10^2\,s^{-1}$ △, M20–$2\times10^{-2}\,s^{-1}$ □, M12–$2.0\times10^3\,s^{-1}$ ●, M12–$5.0\times10^2\,s^{-1}$, ▲, M12–$8\times10^{-2}\,s^{-1}$ ■; (b) $1.5\times10^4\,s^{-1}$ +, $9.0\times10^3\,s^{-1}$ ○, $3.3\times10^2\,s^{-1}$ △, $8.0\times10^{-2}\,s^{-1}$ □; and (c) $2.7\times10^3\,s^{-1}$ +, $1.5\times10^3\,s^{-1}$ ○, $2.2\times10^2\,s^{-1}$ △, $3.5\times10^{-2}\,s^{-1}$ □.

then run until sufficient elements had failed to indicate complete separation. Predicted and measured effective plastic strains and times to fracture are compared in Table III for AQ85 pure iron, mild steel and aluminium alloy, respectively. Although predicted times to fracture are consistently less than measured experimentally, the trends are correctly predicted by the numerical simulations and the agreement is reasonable considering the speed and complexity of the loading conditions. This indicates that the Johnson–Cook fracture model with the constants derived as described above can be used for good estimates of fracture over the range of conditions investigated.

TABLE II Constants of Johnson–Cook fracture model for mild steel, AQ85 iron, aluminium alloy

Material	D_2	D_3
Mild steel	8.54	2.50
AQ85 iron	8.71	1.53
Aluminium alloy	2.03	1.09

5. Discussion

It is apparent from the above results that the ductility of all three materials tested is strongly dependent on the level of stress triaxiality in the specimen as expected. This dependency is greatest for the ferrous materials and least for the aluminium alloy. What is less clear is any obvious strain-rate effect for the results which represents fully ductile failure. This is despite the fact that strain-rate is known to significantly effect the flow stress properties over the range of strain-rates tested. However the use of a strain-rate dependent constitutive relation in numerical simulations of the experiment allows the effect of strain-rate on the stress triaxiality parameter to be taken into account. Any additional strain-rate dependency of the fracture strain would seem to be a second order effect for the materials tested, provided of course that the fracture remains fully ductile.

From the results for mild steel it is clear that the combined effects of strain-rate and stress triaxiality can control the mode of failure. For a given level of stress triaxiality, a transition to a brittle fracture mode is seen to occur as the strain-rate is increased (Table I). This effect was also observed for the as-received pure Remko iron [9] and is analogous to the ductile–brittle transition seen in metals (for constant σ_m/σ_e) as the temperature is reduced. The fact that the failure mode of the AQ85 pure iron remains ductile even for the most severe combinations of stress triaxiality and strain-rate is an indication of the success of the special processing received by this material in maintaining its good ductility over a wide range of conditions.

In view of the lack of clear strain-rate dependency of the ductile fracture results, it is reasonable to ignore the strain-rate term in the semi-empirical fracture model adopted (Equation 7). The other factor effectively ignored is the temperature dependency although there is less evidence at present for this. At high rates of loading (above about $10^2\,s^{-1}$), the deformation can be assumed to be adiabatic which means that the heat generated by the plastic work results in a very rapid temperature rise in the material. This temperature rise can be substantial and is greatest near the site of fracture initiation (typical rises predicted by DYNA2D are 240 °C for iron at a strain of 1.5 and 100 °C for aluminium at a strain of 0.6). The elevated temperature will reduce the material flow stress due to thermal softening and hence will also change the stress triaxiality at the fracture site. However, this effect is again allowed for in the numerical simulations of the experiment (provided the material constitutive relation includes a thermal softening term). The question remains whether there is an additional effect of temperature on the ductile fracture process at high strain-

TABLE III Comparison of predicted and measured fracture times and strains for AQ85 iron, mild steel and aluminium alloy with 28° wedge impacting at 10 ms^{-1}

Material	Notch radius	Fracture times (μs)		Fracture strains	
	(mm)	experiment	numerical	experiment	numerical
AQ85 iron	4	257	219	1.94	1.91
	2	—	181	–	1.53
	1	174	152	1.51	1.22
	0.5	152	141	1.50	0.87
Mild steel	4	168	129	0.65	0.64
	2	133	87	0.25	0.32
	1	135	62	0.16	0.14
	0.5	83	73	0.10	0.21
Aluminium alloy	8	293	145	0.34	0.41
	4	268	115	0.34	0.30
	2	160	95	0.34	0.23
	1	149	92	0.29	0.23
	0.5	164	92	0.25	0.20

rates (over and above that due to changes in the stress field). This question is currently being addressed by further experimental and numerical studies over a range of different test start temperatures, including sub-ambient temperatures down to 500 °C which may be expected to induce a ductile–brittle transition even in the highly ductile AQ85 iron [19].

6. Conclusions

1. The ductility, measured as the effective plastic strain at failure in a notched tensile test, of mild steel, specially-processed pure Remko iron and aluminium alloy BS1474 is strongly dependent on the level of stress triaxiality in the specimen over a wide range of strain-rates (10^{-3} to 10^{4} s^{-1}). This dependency is greatest for the ferrous materials and least for aluminium.

2. No dependency of the ductility on the rate of loading could be determined from the experimental results for the pure iron or aluminium. However, for mild steel, a transition to a brittle mode of fracture was observed under certain test conditions. This transition occurred at a lower level of stress triaxiality at high strain-rates in comparison with specimens tested under quasi-static conditions.

3. When properly interpreted in terms of conditions of stress and strain at the point of fracture initiation (as predicted by numerical simulations of the experiment), the results presented in this paper enable the constants of an empirical ductile fracture model to be determined. This model together with a simple damage accumulation fracture criterion was found to yield estimates of the time and average strain to failure in reasonable agreement with experiment.

4. Despite the success of the fracture modelling studies, further work is required before such models can be used with confidence outside the range of conditions for which they were derived. In particular, the effect of temperature (both elevated and sub-ambient) will form part of a future more extensive study on ductile fracture behaviour.

Acknowledgement

This work was carried out under the UK Defence Research Agency Agreement Number CB/FRN/9/4 /2062/155/RARDE for which support the authors are duly grateful.

References

1. G. R. JOHNSON and W. H. COOK, in Proceedings of the 7th International Symposium on Ballistics, The Hague, April 1983, p. 541.
2. F. J. ZERILLI and R. W. ARMSTRONG, *J. Appl. Phys.* **61** (1987) 1816.
3. B. D. GOLDTHORPE, in Proceedings of DYMAT91 Conference, Strasbourg, Oct. 14–18, 1991. *J. Phys. IV* Coll C3 Vol. 1, p. 829.
4. J. R. RICE and D. M. TRACEY, *J. Mech. Phys. Solids* **17** (1969) 201.
5. J. W. HANCOCK and A. C. MacKENZIE, *ibid.* **24** (1976) 147.
6. G. R. JOHNSON and W. H. COOK, *Eng. Fracture. Mech.* **21** (1985) 31.
7. R. G. WHIRLEY and J. O. HALLQUIST, Lawrence Livemore National Laboratory, Rept. UCRL-MA-110630, 1991.
8. *Idem*, Lawrence Livemore National Laboratory, Rept. UCRL-MA-107254, 1991.
9. H. MAJZOOBI, PhD thesis, Department of Mechanical Engineering, University of Leeds, Leeds (1990).
10. F. A. McCLINTOCK, *Trans. ASME, J. Appl. Mech.* **35** (1968) 363.
11. D. W. BRIDGMAN, "Studies in large plastic flow and fracture" (McGraw Hill, New York, 1952).
12. D. K. BROWN and J. C. EARL, *Eng. Fracture Mech.* **8** (1976) 599.
13. D. P. CLAUSING, *J. Mater.* **4** (1969) 566.
14. A. S. ARGON and A. NEEDLEMAN, *Metall. Trans.*, **6A** (1975) 815.
15. M. S. MIRZA, PhD thesis, Department of Mechanical Engineering, University of Leeds, Leeds (1993).
16. B. ENGELMANN and J. O. HALLQUIST, Lawrence Livemore National Laboratory, Rept. UCRL-MA-105413, 1991.
17. L. SEAMAN, D. R. CURRAN, J. B. AIDUN and T. COOPER, *Nuc. Eng. Des.*, **105** (1987) 35.
18. A. NEEDLEMAN and V. TVERGAARD, *J. Mech. Phys. Solids* **32** (1984) 461.
19. D. C. BARTON, M. S. MIRZA, J. L. STURGES and M. WAHEED, in Proceedings of DYMAT94, Oxford, 1994. *J. de Physique* **4** (1994) p. 659.

Received 9 August 1994
and accepted 22 June 1995